Chemical Science

ROYAL SOCIETY OF CHEMISTRY

EDGE ARTICLE

View Article Online
View Journal

Cite this: DOI: 10.1039/d6sc02475k

All publication charges for this article have been paid for by the Royal Society of Chemistry

Aromatic phosphonate-based luminophores: universal building blocks for ultralong room-temperature phosphorescence and multifunctional applications

Chunli Li, Zizhao Huang, Tao Li, Tengjiao Zhao, Lei Zhou, Zhenyi He,* He Tian and Xiang Ma *

The construction of organic ultralong room-temperature phosphorescence (OURTP) materials with high photoluminescence quantum yield and long lifetime is significant but challenging. Non-radiative transition caused by excessive molecular aggregation and vibrational relaxation usually suppresses phosphorescence of polycyclic aromatic hydrocarbons (PAHs) under ambient conditions. Herein, functionalization of PAHs with diethyl phosphonate has been proven effective in achieving full-color OURTP with stimulus-responsive properties in various polymers. The introduction of hydrophilic substituents significantly inhibits excessive molecular aggregation and phase separation between the host and guest. Non-covalent interactions such as hydrogen bonding and electrostatic interaction can enhance environmental rigidity and hinder vibrational relaxation. The synergistic effect of these interactions greatly suppresses non-radiative transition, unlocking efficient OURTP with long lifetime and high photoluminescence quantum yield of 2.05 s and 41.7% in different doped systems, respectively. Meanwhile, aromatic phosphonate-based luminophores can be uniformly dispersed in the host by switching different hydrophilic and hydrophobic polymers. The extraordinary luminescence performance of the doped systems outperforms other substituents, demonstrating the effectiveness and versatility of diethyl phosphonate functionalization. Furthermore, benefiting from the multi-stimulus response and full-color afterglow of the doped systems, potential applications in anti-counterfeiting, dynamic pattern visualization and 3D printing are explored, providing novel perspectives for the construction and application in OURTP materials.

Received 26th March 2026
Accepted 4th May 2026

DOI: 10.1039/d6sc02475k

rsc.li/chemical-science

Introduction

Organic ultralong room-temperature phosphorescence (OURTP) materials, with unique attributes of long lifetime, large Stokes shifts and excellent modifiability, are attracting tremendous attention in advanced functional materials such as biomedicine, anti-counterfeiting and photodynamic therapy.[1–8] The luminescence lifetime, photoluminescence quantum yield and color are usually considered as important performance parameters in practical application. However, the improvement of performance is primarily constrained by two factors. On the one hand, weak spin–orbit coupling (SOC) leads to low inter-system crossing (ISC) efficiency;[9] On the other hand, sensitive triplet excitons are prone to deactivation due to energy transfer with oxygen and a flexible environment.[10] Traditionally, lanthanide metals and heavy atoms are introduced to promote ISC and generate triplet excitons, but this often suffers from drawbacks including great biotoxicity, high cost and limited processability. Notably, polycyclic aromatic hydrocarbons (PAHs) are viewed as promising and efficient organic luminophores. The large conjugated structure and rigid planar conformation provide possibility for high-performance RTP by reducing non-radiative transition. Furthermore, the modifiability of structure and tunability of electronic distribution can confer diversity in molecular structure, dynamic luminescence and functional applications.[11,12] Although PAHs can launch strong fluorescence, phosphorescence is typically suppressed at room-temperature for non-radiative transition caused by aggregation-caused quenching (ACQ).[13–15] Usually, useful strategies for enhancing environmental rigidity consist of crystallization, polymerization, host–guest complexation and doping.[16–18] Therein, polymer-based OURTP doped materials display promising potential in the field of flexible luminescence materials due to straightforward preparation, minimal dosage of luminophores, excellent flexibility and processability.[19,20]

Key Laboratory for Advanced Materials, Joint International Research Laboratory of Precision Chemistry and Molecular Engineering, Frontiers Science Center for Materiobiology and Dynamic Chemistry, School of Chemistry and Molecular Engineering, East China University of Science and Technology, Shanghai 200237, China. E-mail: maxiang@ecust.edu.cn; zhenyiheh@qq.com

Host polymers such as polymethyl methacrylate (PMMA) and polyacrylonitrile (PAN) exhibit pronounced hydrophobic properties, necessitating guest molecules with oil solubility to ensure uniform dispersion for suppressing ACQ.[21,22] Nevertheless, oil-soluble luminophores often undergo excessive aggregation in hydrophilic polymers such as polyvinyl alcohol (PVA) due to differences in hydrophilicity and hydrophobicity, which would enhance intermolecular π–π stacking and non-radiative transition, thereby triggering phase separation and significantly reducing luminescence properties.[23–25] Through precise molecular engineering, hydrophilic functional groups are introduced into PAHs to build a local hydrophilic microenvironment, thereby preventing the occurrence of excessive aggregation and phase separation. Simultaneously, hydrophilic groups including heteroatoms such as phosphorus and oxygen could serve as excellent hydrogen bonding acceptors to form strong hydrogen bonding and stabilize triplet excitons.[26–31] The introduction of hydrophilic functional groups enables researchers to design structures at the molecular level and endows OURTP materials with extended functional properties, holding great promise for developing high-performance OURTP systems.

Here, aromatic phosphonate-based luminophores were doped in various polymers by physical doping to successfully construct high-performance OURTP materials with stimulus-responsive and full-color tunability. With changes in molecular conjugation, different doped systems achieved broadband OURTP emission spanning from blue to red.[32–34] The luminous lifetime and photoluminescence quantum yield of different doped systems reached up to 2.05 s and 41.7%, respectively. Meanwhile, the doped systems exhibited stimulus-responsive characteristics to temperature, photoactivation and excitation wavelength. By switching the host between hydrophilic and hydrophobic polymers, results showed that doped system containing aromatic phosphonate-based luminophores exhibited uniform luminescence, with superior luminescence performance compared to doped systems with other substituent groups. Analysis revealed that the local hydrophilic microenvironment substantially suppresses ACQ caused by excessive aggregation of luminophores and phase separation.[35–38] At the same time, non-covalent interactions such as hydrogen bonding and electrostatic interaction between the host and guest can strengthen the environment rigidity and inhibit vibrational relaxation.[39–42] Synergistic effects of these interactions greatly promoted high-performance OURTP. Efficient luminescent properties enable the doped systems to possess great application potential in information encryption, anti-counterfeiting and 3D printing, paving a viable pathway for developing innovative and high-performance luminescent materials.

Results and discussion

A series of aromatic phosphonate-based luminophores were synthesized *via* a one-step reaction, named BPP, NaP, PheP and PyP. The structures of luminophores were characterized by ^{1}H NMR, ^{13}C NMR and high-resolution mass spectroscopy (Fig. S1–S12). High-performance liquid chromatography (HPLC) was employed to determine the purity of luminophores, thus avoiding the luminescence effect of impurities (Fig. S13). The 2-methyltetrahydrofuran solutions of four luminophores all exhibited distinct delayed emission at 77 K, indicating that four luminophores have giant potential for achieving OURTP in a rigid environment under ambient conditions[43] (Fig. S14). Subsequently, PVA was selected as the host matrix, whose molecular chains contain abundant hydroxyl groups (–OH)

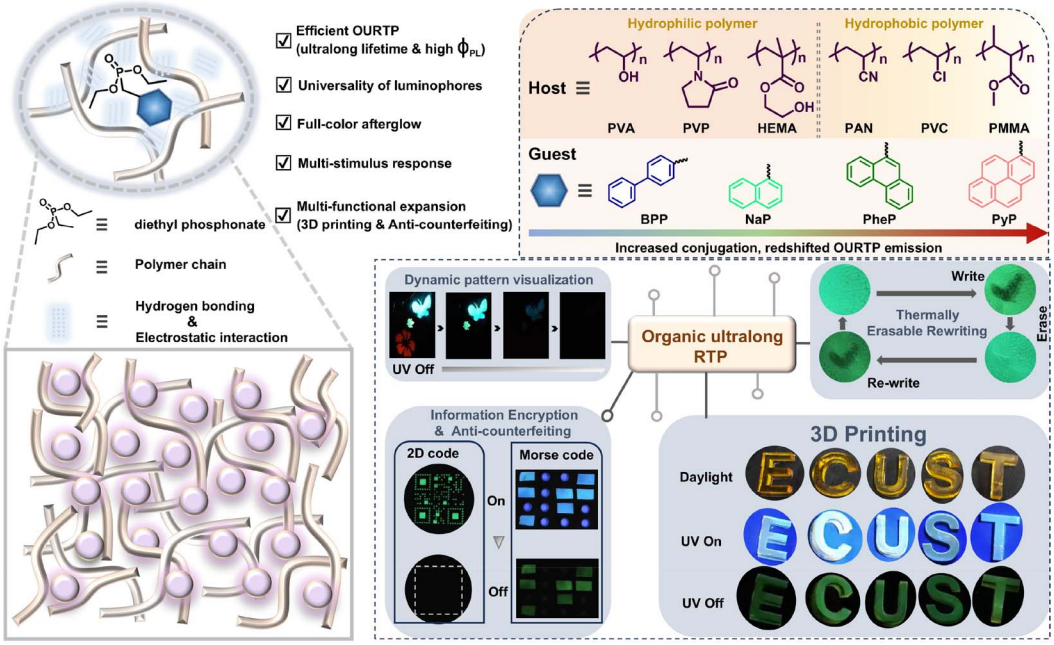

Scheme 1 Schematic illustration of the doped systems, molecular structures and applications.

allowing solid hydrogen-bond formation with luminophores.[44–47] Doped systems were obtained by simply mixing the luminophores and host in a 323 K aqueous solution followed by solvent evaporation and thermal annealing at 393 K for 30 minutes, termed BPP-PVA, NaP-PVA, PheP-PVA and PyP-PVA (Scheme 1).

The luminescence behaviours of the doped systems with different doping mass concentrations were first investigated (Fig. S15–S17). The results suggested that the doped systems maintained strong OURTP even at a low mass concentration of 0.01 wt%. As the doping mass concentration increased, emission peaks and absorption spectra of the four doped systems all showed a gradual red shift trend (Fig. S18). The UV-vis absorption spectra of the four luminophores are shown in Fig. S19. Taking luminescence intensity and lifetime of the doped system into consideration, optimal doping mass concentrations were determined to be 0.1 wt% for BPP-PVA and PheP-PVA, and 0.3 wt% for NaP-PVA and PyP-PVA, respectively.

The four doped systems, BPP-PVA, NaP-PVA, PheP-PVA and PyP-PVA, displayed obvious fluorescence peaks around 320 nm, 340 nm, 373 nm and 396 nm, respectively (Fig. S20). As shown in Fig. 1a, the delayed emission spectra of the four doped systems displayed emission peaks at 480 nm, 525 nm, 510 nm and 605 nm at room temperature, respectively. The luminescence color spanned the entire visible spectrum from blue to red, and the corresponding lifetimes of delayed emission reached up to 2.05 s, 1.26 s, 1.94 s and 0.32 s (Fig. 1b). Upon cessation of UV light, all four films exhibited long-lived bright emission, manifesting as visible afterglow (Fig. 1f). Both the long lifetime and large Stokes shift verified the phosphorescence properties of delayed emission in the four doped systems.[48–50] Moreover, low temperature can suppress non-radiative transition led by free molecular motion, thereby resulting in reinforced emission intensity and longer lifetime.[51,52] For BPP-PVA, the lifetime of delayed emission at 480 nm extended from 0.14 s to 2.92 s, accompanied by an increasing tendency of emission intensity when the temperature declined from 317 K to 77 K. This phenomenon could be regarded as a typical phosphorescence property of the four doped systems (Fig. 1d and e).

It is worth noting that delayed emission peaks of BPP-PVA, NaP-PVA and PyP-PVA at room-temperature also correspond to delayed emission spectra of luminophores in dilute solutions at 77 K (Fig. S14), confirming that delayed emission originated form intrinsic phosphorescence of individual luminophores.[53] After cessation of ultraviolet (UV) irradiation, the four doped systems exhibited visible long afterglow with different colors. Besides, the afterglow duration of BPP-PVA and PheP-PVA exceeded 10 s (Fig. 1f). Photoluminescence quantum yields of the doped systems are shown in Fig. 1c, revealing that BPP-PVA, NaP-PVA, PheP-PVA and PyP-PVA exhibited efficient yields up to 15.9%, 9.0%, 21.4% and 41.7%, respectively. These results demonstrated the feasibility of diethyl phosphonate functionalization, and luminophores were then incorporated into the PVA rigid matrix to obtain excellent OURTP materials with long lifetime and high photoluminescence quantum yield.

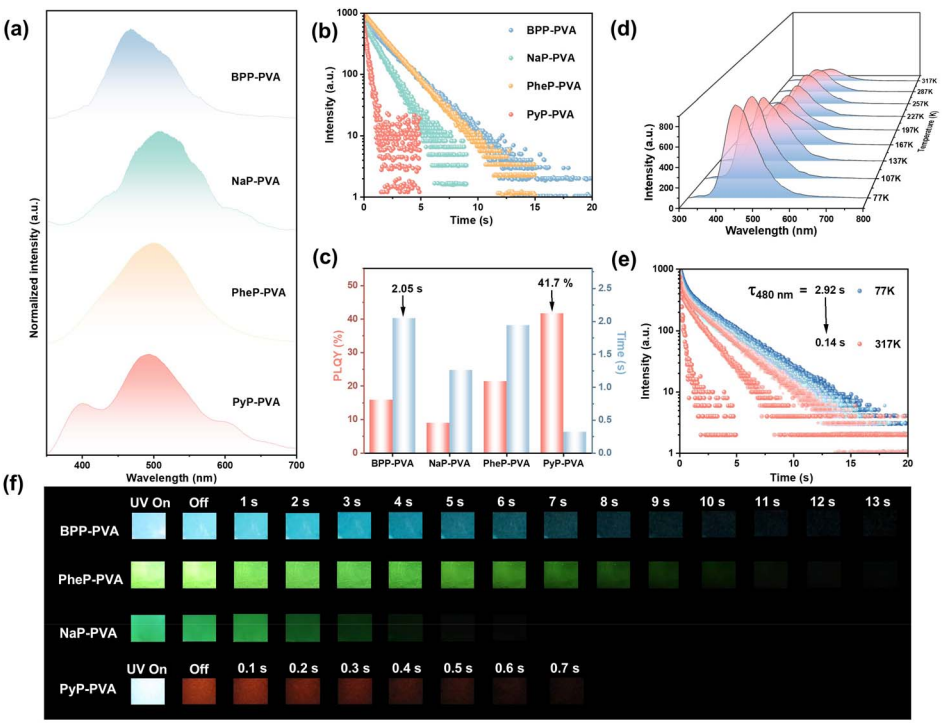

Fig. 1 (a) Delayed emission spectra and (b) lifetime decay curves of BPP-PVA (λ_{ex} = 254 nm), NaP-PVA (λ_{ex} = 280 nm), PheP-PVA (λ_{ex} = 250 nm) and PyP-PVA (λ_{ex} = 305 nm); (c) photoluminescence quantum yield and phosphorescence lifetime values of the doped systems; (d) temperature-dependent delayed emission and (e) lifetime decay curves of BPP-PVA (λ_{ex} = 254 nm); (f) photographs of the luminescence of the doped systems (delay time = 0.1 ms).

To gain deeper insight into the luminescence mechanism of efficient OURTP in the doped systems, relevant characterization and theoretical calculations were performed on the four doped systems. First, X-ray powder diffraction (XRD) was used to analyse the microstructure of the doped systems. The results showed no obvious crystal characteristics and verified amorphous states of the doped systems (Fig. 2a).

Given that the doped systems were amorphous, we speculated that efficient OURTP was promoted by non-covalent interactions between the PVA matrix and luminophores, such as hydrogen bonding and electrostatic interaction. Therefore, Fourier transform infrared (FT-IR) spectroscopy was employed to confirm our hypothesis. PheP-PVA was selected as the research example. The vibration peak of the –OH group was located at 3253 cm^{-1} in the pure PVA matrix. However, the vibration peak of the film doped with 0.1 wt% PheP shifted to 3267 cm^{-1}. Then, as the doping mass concentration of PheP was gradually increased to 10 wt%, the –OH vibration peak of PheP-PVA underwent a 24 cm^{-1} displacement and shifted to 3277 cm^{-1}, which clearly demonstrated the hydrogen bonding between the PVA matrix and luminophores[54] (Fig. 2d). Furthermore, differential scanning calorimetry (DSC) analysis showed that the glass transition temperature of the pure PVA matrix was 100.74 °C, while the doped system PheP-PVA displayed a higher glass transition temperature, implying the appearance of strong interactions occurred in the PVA chain and luminophores[55] (Fig. 2b). Additionally, PAHs without diethyl phosphonate functionalization were doped in the PVA matrix, named Na-PVA, BP-PVA, Phe-PVA and Py-PVA, and we tested the corresponding photophysical properties. Compared with films doped with aromatic phosphonate-based luminophores, doped films without diethyl phosphonate functionalization significantly exhibited lower photoluminescence quantum yield and shorter lifetime (Fig. 2e and S21). This was because P and O atoms in diethyl phosphonate could form hydrogen bonding with –OH in the PVA chain, thereby inhibiting non-radiative transition induced by free molecular motion and enhancing phosphorescence performance[56] (Fig. 2c).

Meanwhile, density-functional theory calculations were applied to obtain the electrostatic potential (ESP) distributions on the surfaces of PVA and the four luminophores for characterizing electrostatic interactions (Fig. 2g). The four luminophores exhibited negative ESP values in phosphine carbonyl moieties, which can be attributed to the strong electron-withdrawing capability. In contrast, the hydrogen atoms of the –OH groups in pure PVA demonstrated strong electron-

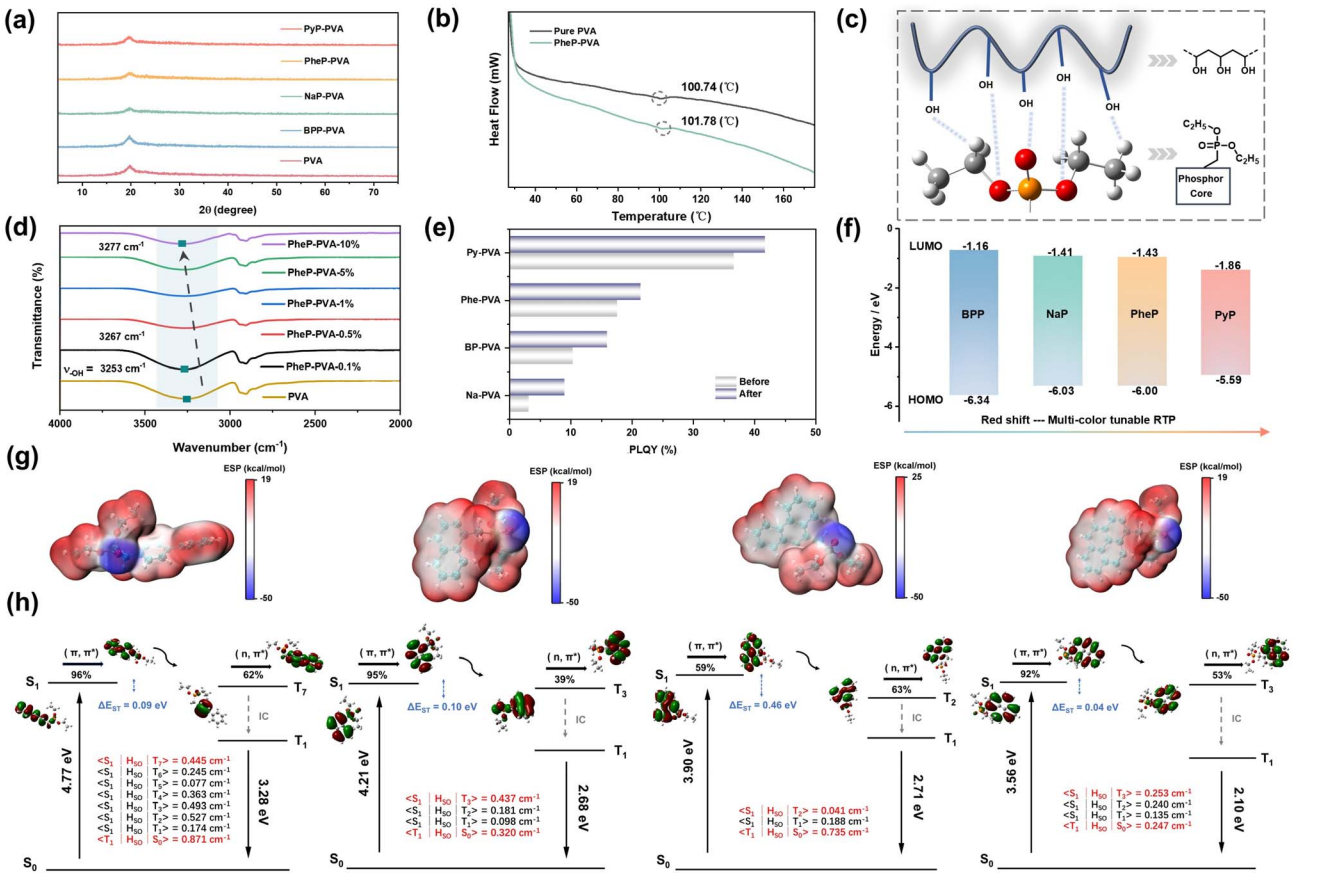

Fig. 2 (a) Powder XRD patterns of BPP-PVA, NaP-PVA, PheP-PVA and PyP-PVA; (b) DSC of pure PVA and PheP-PVA; (c) brief illustration of hydrogen bonding; (d) FT-IR spectra of PVA and PheP-PVA with different mass ratios of luminophore; (e) photoluminescence quantum yield of the doped systems before and after diethyl phosphonate functionalization; (f) Frontier molecular orbital analysis, (g) ESP distribution and (h) energy level distributions of BPP, NaP, PheP and PyP.

donating ability due to the electron push–pull effect (Fig. S22). When luminophores contacted PVA chains in the doping environment, a strong electrostatic interaction would happen because the existence of the phosphine carbonyl moiety with electron-withdrawing capability was complementary to the electron-donating portion in the PVA chain.[57,58] The microenvironment around luminophores became more rigid, which helped reduce non-radiative transition and prolonged lifetime.

At the same time, density-functional theory (DFT) and time-dependent density-functional theory (TD-DFT) calculations were also used to evaluate the ground-state and excited-state geometry, the highest occupied molecular orbital (HOMO), the lowest unoccupied molecular orbital (LUMO) and energy level distributions. From the perspective of electronic conformation, the S_1 states of the four luminophores were dominated by π–π* transitions from the HOMO to the LUMO (Fig. 2h). For luminophore PheP, 63% n–π* transition appeared in the T_2 level. BPP exhibited 62% n–π* transition in the T_7 level. According to the EI-Sayed rule,[59] the occurrence of different transitions is permitted. Hence luminophores had giant potential for achieving efficient OURTP. The data revealed that NaP exhibited an energy gap of 0.0995 eV from S_1–T_3 with a SOC constant of 0.437 cm^{-1}. A smaller singlet–triplet energy gap and a larger SOC constant of aromatic phosphonate-based luminophores led to a pronounced ISC process, thereby promoting OURTP performance[27] (Fig. 2f and Table S1). The HOMO–LUMO energy gap of BPP and PyP was 5.18 eV and 3.73 eV, respectively. The gradually decreasing HOMO–LUMO energy gaps from BPP to PyP simultaneously demonstrated that OURTP of the doped systems can be redshifted from blue to red, spanning the visible spectrum[7] (Fig. 2f). The energy gap of the four luminophores without diethyl phosphonate functionalization showed the same trend, and theoretical calculations are consistent with the experimental phenomenon (Fig. S23). Therefore, the rigid environment formed by strong non-covalent interactions between the PVA matrix and aromatic phosphonate-based luminophores was responsible for efficient OURTP. Besides, PheP was selected as the template molecule to be doped into various host matrices. Experimental results revealed that doped systems containing PheP still exhibited long and efficient OURTP (Fig. S24 and S25), further verifying the universal applicability of aromatic phosphonate-based luminophores across different host matrices.

The planar conjugated structure of unmodified PAHs endows the molecule with appreciable rigidity and potential to achieve efficient OURTP with full-color tunability. However, the hydrophobic nature frequently triggers phase separation when luminophores are dispersed in hydrophilic polymers, thus leading to excessive aggregation, non-radiative transition caused by π–π stacking and quenching phosphorescence.[11] Therefore, molecular engineering was employed to modify PAHs with diethyl phosphonate. The polarity of diethyl phosphonate enabled luminophores to form hydrogen bonding with water molecules, creating a local hydrophilic microenvironment. The presence of ethyl groups also increased steric hindrance, urging more dispersed distribution of luminophores in the host and improving phosphorescence performance.

To verify the rationality of diethyl phosphonate functionalization, a luminophore named NaM without diethyl phosphonate functionalization was doped in both hydrophilic and hydrophobic polymers to make a comparison with doped systems containing NaP (Fig. 3a). The fluorescence spectra and photoluminescence spectra of NaM solution both displayed an obvious emission peak around 305 nm. But NaM solution showed no delayed emission under ambient conditions, which was caused by the relatively low rigidity of the environment and the quenching effect of water and oxygen (Fig. S26). The UV-vis absorbance spectra of NaM solution are presented in Fig. S27. Moreover, it could be seen that the distributions of NaM and NaP were uniform in hydrophobic polymers. For example, the mixture of NaP and PMMA was homogeneous and transparent after ultrasonication at 323 K for 1 h (Fig. 3d). After solvent evaporated tardily, the surface of the doped systems appeared exceptionally smooth and flat. Energy-dispersive X-ray spectroscopy (EDS) images revealed uniform P distribution throughout the doped systems without any excessive aggregation clumps (Fig. 3e). This result stemmed from the inherent lipophilic nature of the benzene ring in luminophores, enabling uniform distribution of luminophores with the hydrophobic host in an organic solvent. In other hydrophobic hosts such as PAN and poly (vinyl chloride) (PVC), doped systems containing NaP all exhibited visible afterglow (Fig. 3f). Next, PVA, polyvinyl pyrrolidone (PVP) and poly (2-hydroxyethyl methacrylate) (HEMA) were selected as hydrophilic hosts. The mixture of NaM-PVA remained cloudy and opaque after ultrasonication at 323 K for 1 h (Fig. 3b). After solvent evaporated naturally, excessive aggregation clumps were observed in scanning electron microscopy (SEM) images, indicating uneven distribution of luminophores in PVA. But the mixed solution of NaP-PVA became homogeneous and transparent after ultrasonication at 323 K for 1 h (Fig. 3c). NaP-PVA exhibited a smooth and uniform surface under SEM observation, with no large excessive aggregation clumps. EDS results revealed uniform distribution of P, implying concomitant diminution of phase separation and excessive aggregation happened in luminophores (Fig. 3e). The above results suggested that aromatic phosphonate-based luminophores displayed highly uniform dispersion and luminescence in both hydrophilic and hydrophobic polymers, avoiding phase separation and excessive aggregation of luminophores (Fig. S28).

Subsequently, we tested delayed emission spectra and lifetime of 1-methylnaphthalene (NaM) and NaP by switching the host. Delayed emission spectra of NaM and NaP in different hosts all displayed an emission peak at 525 nm, with visible green afterglow at room-temperature. However, the lifetimes of systems doped with NaP consistently exceeded those of systems doped with NaM (Fig. S29–S32). Taking hydrophilic host PVP as an example, NaM-PVP showed a short lifetime of 1.34 ms, whereas the lifetime of NaP-PVP reached up to 566.28 ms, prolonging by 422-fold (Fig. 3g and h). In hydrophobic host PMMA, NaP-PMMA exhibited a long lifetime of 446.9 ms after

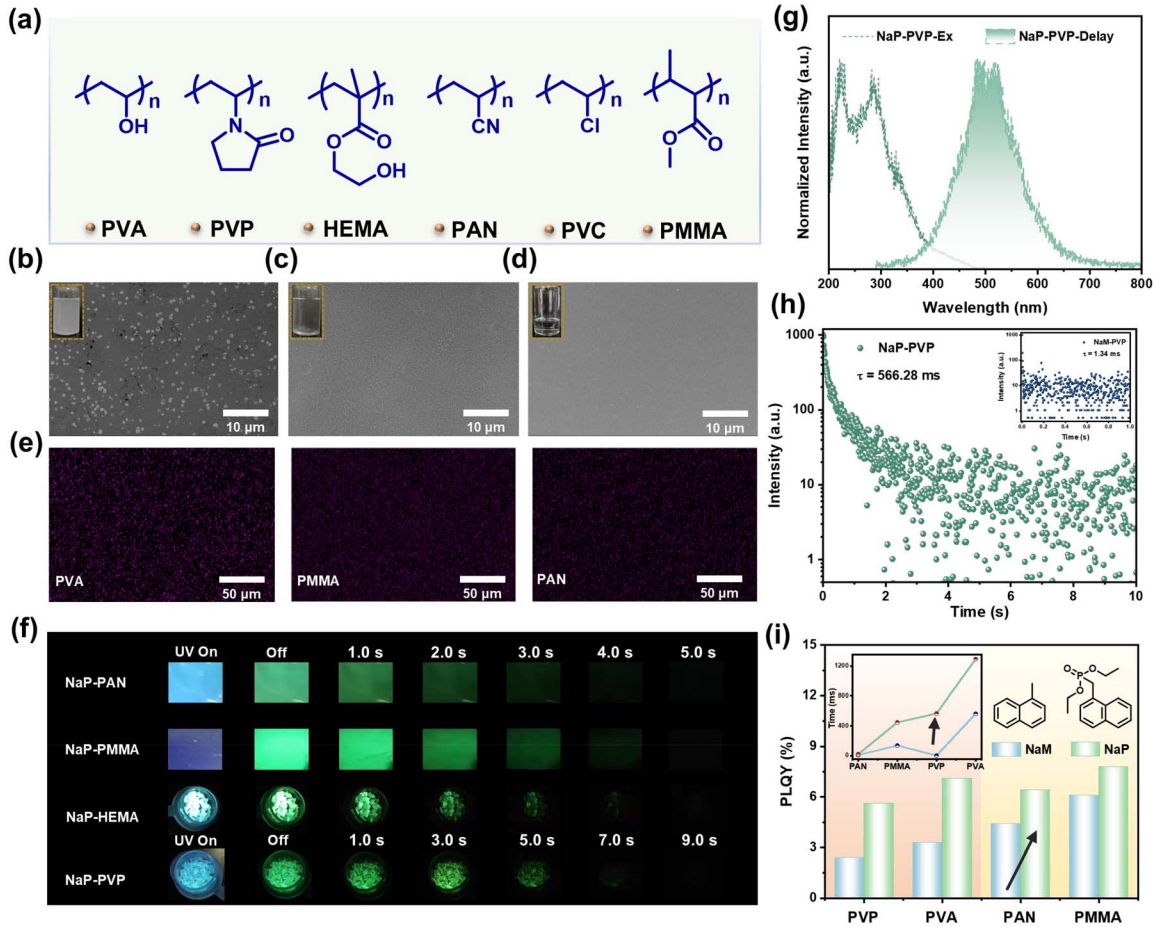

Fig. 3 (a) Chemical structures of polymers; SEM images of (b) NaM-PVA, (c) NaP-PVA and (d) NaP-PMMA; (e) EDS mapping of the P element in the doped systems; (f) photographs of luminescence of the doped systems; (g) excitation spectra and delayed emission spectra of NaP-PVP; (h) lifetime decay curves of NaM-PVP (λ_{ex} = 280 nm) and NaP-PVP (λ_{ex} = 280 nm); (i) photoluminescence quantum yield and lifetime of the doped systems. All tests were conducted at 25 °C under ambient conditions.

photoactivation, while NaM-PMMA only showed a lifetime of 136.46 ms after photoactivation.

Furthermore, photoluminescence quantum yields of systems doped with NaP were higher than that of systems doped with NaM in both hydrophilic and hydrophobic polymers (Fig. 3i), implying that diethyl phosphonate functionalization prevented the excessive aggregation and facilitated uniform distribution of luminophores in the host. Consequently, the synergistic effects of non-covalent interactions such as hydrogen bonding and electrostatic interaction enhanced microenvironment rigidity, promoting OURTP performance in terms of lifetime and photoluminescence quantum yield.

Additionally, four different hydrophilic functional groups—carboxyl (–CA), amino (–NH), sulfonic acid (–SA) and boric acid (–BA)—were used to modified Na, named Na–BA, Na–SA, Na–CA and Na–NH. These luminophores were doped into PVA to construct doped films, and their photophysical properties were analysed. The results showed that all doped films achieved obvious emission at 525 nm with lifetime below 1 s. Visible green afterglow was observable at room-temperature after turning off UV light. Comparing phosphorescence performance of these four doped systems with that of NaP-PVA, NaP exhibited the longest lifetime, and its photoluminescence quantum yield was second only to that of Na–BA–PVA. These findings suggested that doped systems containing aromatic phosphonate-based luminophores afforded the overall best phosphorescence performance, surpassing other hydrophilic functional group-substituted luminophores[60] (Fig. S33). Given that non-covalent interactions were highly sensitive to environmental changes and can respond promptly, we investigated the stimulus-responsive properties of the doped systems. The influence of temperature variation on the luminescence of the doped systems was studied. As temperature increased from 293 K to 333 K, afterglow duration of PheP-PVA gradually decreased from 13 s (Fig. 4g). We speculated that high temperature would destroy hydrogen bonding between PVA and luminophores, reducing the rigidity of the microenvironment around luminophores and decreasing phosphorescence performance. FT-IR spectroscopy was employed to confirm this variation (Fig. 4a). The vibration peak of PheP-PVA at 3436 cm^{-1} indicated the appearance of hydrogen bonding between PVA and PheP. When the temperature increased to 333 K, the intensity of the

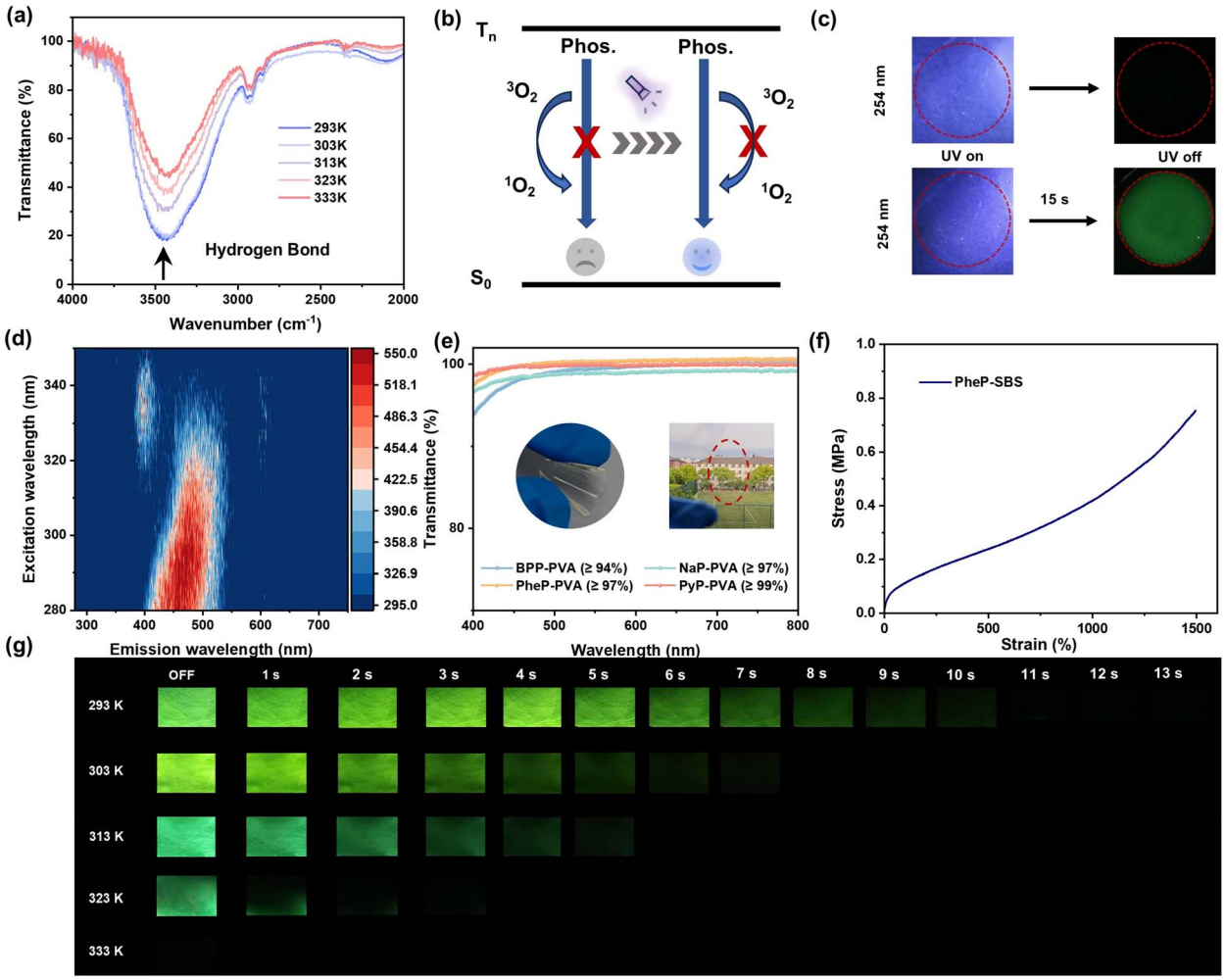

Fig. 4 (a) Temperature-dependent FT-IR spectra and (g) afterglow photographs of PheP-PVA (λ_{ex} = 254 nm); (b) the diagram of the internal mechanism of oxygen consumption; (c) photographs of PheP-PMMA under UV irradiation; (d) excitation–emission mapping of PyP-PVA; (e) transmittance spectra of BPP-PVA (thickness = 0.10 mm), NaP-PVA (thickness = 0.10 mm), PheP-PVA (thickness = 0.10 mm) and PyP-PVA (thickness = 0.10 mm). Inset: photographs of NaP-PVA; (f) stress–strain curves of PheP-SBS.

vibration peak diminished, and the position shifted to 3418 cm^{-1}. This change confirmed that hydrogen bonding between the host and luminophores weaken with increasing temperature, reducing the rigidity of the doped environment.[61] Acceleration of non-radiative transition directly led to the decline of OURTP.

Next, the response properties of PheP-PMMA under photoactivation were investigated. After turning off UV light, PheP-PMMA without photoactivation showed no afterglow. Upon 15 s continuous photoactivation at 254 nm, PheP-PMMA exhibited vivid green afterglow after cessation of UV irradiation (Fig. 4b and c). It has been reported that PMMA can create a relatively rigid microenvironment for luminophores but is prone to oxygen permeation, which easily quenches triplet excitons and declines OURTP. To determine potential photoactivation mechanisms, delayed emission spectra of PheP-PMMA under argon and air were measured (Fig. S34). In air, PheP-PMMA showed no significant emission after stopping UV irradiation, and lifetime was difficult to detect. Nevertheless, PheP-PMMA in an argon environment displayed a strong emission peak at 510 nm after stopping UV irradiation. During the process of photoactivation, UV light would gradually deplete oxygen.[62] Then, sensitive triplet excitons were successfully released and emitted phosphorescence.

It is well known that doped systems containing Py can exhibit concentration-dependent properties.[63] As a result, PyP-PVA was chosen as the research subject to explore phosphorescence performance. Upon increasing the excitation wavelength, phosphorescence emission of PyP-PVA gradually underwent a red shift (Fig. 4d). Analogous to concentration dependence, wavelength dependence of excitation originated from the formation of aggregates, causing an overall red shift in excitation and emission wavelengths of the doped systems. Besides, all doped films owned high transparency and flexibility. For hydrophilic polymer PVA, the transmittance rates of PheP-PVA and NaP-PVA were as high as 97% among the range of 400 nm-800 nm, while PyP-PVA surpassed 99% (Fig. 4e). The doped films with hydrophobic polymers also exhibit high

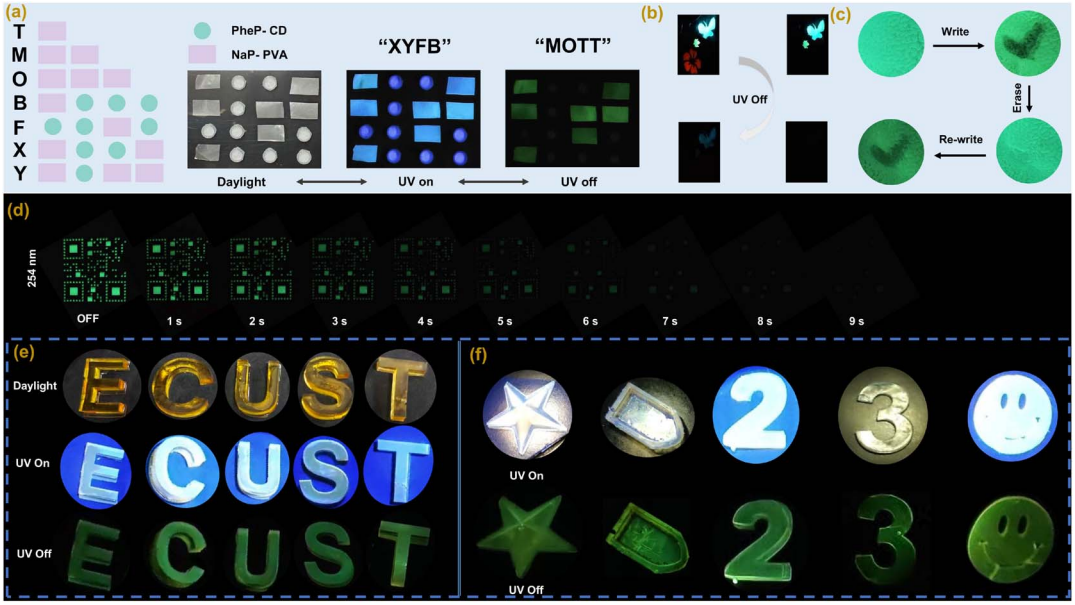

Fig. 5 (a) Information encryption with Morse code (PheP-CD and NaP-PVA); (b) dynamic display of patterns (BPP-PVA, PheP-PVA and PyP-PVA); (c) schematic illustration of the application process for the PheP-PVA rewritable doped system; (d) 2D code imaging based on PheP-PVA; (e) and (f) photographs of 3D RTP materials under daylight, UV excitation and after switching off.

transparency. For instance, the transmittance rates of both NaP-PMMA and NaP-PVC exceeded 90% in the wavelength range above 400 nm (Fig. S35). Furthermore, PheP showed favorable mechanical properties in a block-copolymer host such as isoprene-styrene (SBS). PheP-SBS withstood tensile stress up to 0.75 MPa while sustaining elongations approaching 1500% (Fig. 4f). To sum up, different doped systems achieved efficient OURTP with high photoluminescence quantum yield and lifetime up to 41.7% and 2.05 s, respectively. The luminescence color covered the visible spectrum from blue to red, and the multi-stimulus response endowed the doped materials with broad application prospects.

Based on efficient OURTP of the doped systems, we explored feasible application in the field of information encryption. PheP-CD and NaP-PVA presented circular and rectangular shapes, respectively. Under daylight, we arranged the two doped materials in a specific sequence. Leveraging the different afterglow duration time of the two doped materials after stopping UV irradiation, information was stored and encrypted with the aid of Morse code. Under UV light at 254 nm, PheP-CD and NaP-PVA both emitted blue fluorescence, storing information "XYFB". Upon removing UV light, NaP-PVA blocks exhibited green afterglow, revealing real information "MOTT" (Fig. 5a). Additionally, the discrepancy in afterglow lifetime and color among the doped systems was applied to dynamic pattern visualization. After removing UV light, red flowers, green leaves and blue butterflies could be observed. Due to the short afterglow of PyP-PVA, red flowers disappeared first, leaving only leaves and butterflies. With time progressed, patterns of leaves and butterflies gradually dimmed until they vanished completely (Fig. 5b). We placed a PheP-PVA film beneath a QR code plate. The green QR code pattern became clear after the removal of UV light, and then faded overtime (Fig. 5d). Benefitting from the sensitive nature of the doped systems to temperature and water, we employed water as an ink for erasable writing on the surface of the doped film. Pattern "√" was written on the surface of PheP-PVA using water. Heating could erase this pattern, and this process was repeatable (Fig. 5c).

Using 3D printing technology, we uniformly dispersed NaP in thermosetting resin at low doping concentration and successfully fabricated 3D materials with OURTP properties. The letter "E", number "2" and five-pointed star pattern were printed, demonstrating the practical formability. Under UV irradiation, all printed 3D structures displayed spontaneous blue fluorescence. Turning off UV light, 3D structures showed green afterglow (Fig. 5e and f). Therefore, doped materials with aromatic phosphonate-based luminophores hold great application potential in functional materials.

Conclusions

In summary, through physical doping, four aromatic phosphonate-based luminophores with distinct conjugated structures were respectively doped into various polymers to successfully construct efficient OURTP materials with multi-stimulus response and full-color tunability. The incorporation of hydrophilic diethyl phosphonate facilitated the formation of a local hydrophilic microenvironment, preventing excessive aggregation and promoting uniform dispersion of luminophores. Meanwhile, vibrational relaxation was greatly suppressed by the rigid environment induced by non-covalent interactions such as hydrogen bonding and electrostatic interaction. Consequently, the synergistic effect of these two mechanisms was responsible for significant improvement of

phosphorescence performance in doped systems. The high photoluminescence quantum yield of 41.7% and long lifetime up to 2.05 s could be simultaneously implemented in different doped systems. Benefiting from the local hydrophilic nature of aromatic phosphonate-based luminophores, the molecules displayed excellent adaptability and uniform distribution in both hydrophilic and hydrophobic polymers, releasing high-performance OURTP. Furthermore, outstanding stimulus-response properties of the doped systems to temperature, excitation wavelength and photoactivation enabled promising applications in anti-counterfeiting, dynamic pattern visualization and 3D printing. This work provides new insights for the construction and application expansion of high-performance OURTP materials.

Author contributions

C. Li, Z. He, H. Tian and X. Ma designed the materials and conceived the project. C. Li conducted the molecule synthesis and characterization. T. Li performed the theoretical calculation. C. Li and X. Ma wrote the manuscript. All authors engaged in discussion and conducted data analysis.

Conflicts of interest

There are no conflicts to declare.

Data availability

All the data are available in the supplementary information (SI). Supplementary information: materials, synthetic routes of compounds, ^{1}H NMR spectra, ^{13}C NMR specra, HRMS spectra, photophysical properties and general methods. See DOI: https://doi.org/10.1039/d6sc02475k.

Acknowledgements

We gratefully acknowledge the financial support from the National Natural Science Foundation of China (22125803, T2488302, and 22408106), the Science and Technology Commission of Shanghai Municipality (24DX1400200), the Guangxi Department of Science and Technology (AA23062016), the Shanghai Rising Star Program (24YF2708500), and the Fundamental Research Funds for the Central Universities.

References

1 C. Yin, Z. Wu, Z. Yan, P. Jiang, Y. Ding, T. Li, Y. Chen, H. Tian and X. Ma, *J. Am. Chem. Soc.*, 2025, **147**, 43286–43294.
2 W. Ye, H. Ma, H. Shi, H. Wang, A. Lv, L. Bian, M. Zhang, C. Ma, K. Ling, M. Gu, Y. Mao, X. Yao, C. Gao, K. Shen, W. Jia, J. Zhi, S. Cai, Z. Song, J. Li, Y. Zhang, S. Lu, K. Liu, C. Dong, Q. Wang, Y. Zhou, W. Yao, Y. Zhang, H. Zhang, Z. Zhang, X. Hang, Z. An, X. Liu and W. Huang, *Nat. Mater.*, 2021, **20**, 1539–1544.
3 X. Zhou, H. Zhang and Y. Liu, *Chem. Sci.*, 2024, **15**, 18259–18271.
4 N. Li, Y. Wang, S. Chen, J. Li and Z. Li, *Angew. Chem., Int. Ed.*, 2025, **64**, e202520504.
5 H. Hou, H. Wang, M. He, Q. Li, X. Wang, F. Guo, Q. Chen, L. Qu and C. Yang, *Angew. Chem., Int. Ed.*, 2024, **63**, e202411323.
6 X. Li, J. Li, G. Wang, Y. Su, M. Wu and K. Zhang, *Nat. Commun.*, 2025, **17**, 226.
7 Z. He, J. Song, C. Li, Z. Huang, W. Liu and X. Ma, *Adv. Mater.*, 2025, **37**, 2418506.
8 W. Zhao, Z. He and B. Tang, *Nat. Rev. Mater.*, 2020, **5**, 869–885.
9 Z. Yan, C. Yin, H. Tian and X. Ma, *Angew. Chem., Int. Ed.*, 2025, **64**, e202417397.
10 J. Cao, J. Song, Y. Hu, F. Zhang and X. Ma, *CCS Chem.*, 2025, **7**, 2065–2074.
11 Y. Liang, P. Hu, H. Zhang, Q. Yang, H. Wei, R. Chen, J. Yu, C. Liu, Y. Wang, S. Luo, G. Shi, Z. Chi and B. Xu, *Angew. Chem., Int. Ed.*, 2024, **63**, e202318516.
12 Y. Jiang, C. Zhang, R. Wang, Y. Lei, W. Dai, M. Liu, H. Wu, Y. Tao and X. Huang, *Adv. Optical Mater.*, 2024, **12**, 2302482.
13 H. Chen, Y. Zhang, J. Shan, M. Dong, Z. Qian, A. Lv, H. Qian, H. Ma, Z. An, L. Gu and W. Huang, *Angew. Chem., Int. Ed.*, 2025, **64**, e202500610.
14 Y. Zuo, X. Wang and D. Wu, *J. Mater. Chem. C*, 2019, **7**, 14555–14562.
15 R. Feng, H. Lv and Q. Song, *Angew. Chem., Int. Ed.*, 2026, **65**, e16177.
16 Z. Huang, Z. He, B. Ding, H. Tian and X. Ma, *Nat. Commun.*, 2022, **13**, 7841.
17 J. Yu, H. Yu, J. Niu, Z. Lei and Y. Liu, *Nano Lett.*, 2024, **24**, 16124–16131.
18 H. Hu, X. Cheng, Z. Ma, Q. Yang, P. Sijbesma Rint and Z. Ma, *CCS Chem.*, 2023, **6**, 1798–1809.
19 Y. Huang, Y. Liu, X. Zheng, J. Wu, Q. Ling and Z. Lin, *Adv. Optical Mater.*, 2025, **13**, 2500743.
20 N. Li, X. Yang, B. Wang, P. Chen, Y. Ma, Q. Zhang, Y. Huang, Y. Zhang and S. Lü, *Adv. Sci.*, 2024, **11**, 2404698.
21 R. Liu, C. Liu, C. Fu, Z. Zhu, K. Chen, C. Li, L. Wang, Y. Huang and Z. Lu, *Angew. Chem., Int. Ed.*, 2024, **63**, e202312534.
22 H. Wu, D. Wang, Z. Zhao, D. Wang, Y. Xiong and B. Tang, *Adv. Funct. Mater.*, 2021, **31**, 2101656.
23 W. Wen, P. Ze, Z. Min and Q. Ming, *Chem. Eng. J.*, 2024, **495**, 153443.
24 R. Tian, S. Xu, Q. Xu and C. Lu, *Sci. Adv.*, 2020, **6**, eaaz6107.
25 Z. Xu, Y. Huang, S. Sun, P. Wang, Z. He, H. Tian and X. Ma, *Angew. Chem., Int. Ed.*, 2025, **64**, e202518340.
26 T. Heidi, P. Dominik L, G. Max, A. Tim, S. Annika, L. Marine, X. Feng and R. Sebastian, *Adv. Mater.*, 2020, **32**, 2000880.
27 X. Zhang, Z. Gong, J. Sun, M. Wang, X. Ding and H. Xu, *Angew. Chem., Int. Ed.*, 2026, **65**, e23525.
28 J. Li, J. Zhang, Y. Ju, Z. Zhou, S. Liu, Y. Ma and Q. Zhao, *Adv. Optical Mater.*, 2026, **14**, e02364.
29 Z. Chi, D. Li, Y. Meng, Z. Qiao, J. Yang, J. Zhou, X. Liu and Z. Li, *Sci. China Chem.*, 2026, **69**, 413–419.
30 S. Sun, L. Ma, J. Wang, X. Ma and H. Tian, *Natl. Sci. Rev.*, 2022, **9**, nwab085.

31 Z. Guan, Z. Tang, Z. Yao, Q. Guo, S. Zhang, Z. Lv, X. Zhang, N. Ma, X. Liu and Z. Hu, *Adv. Mater.*, 2025, **37**, e07192.
32 D. Li, J. Yang, M. Fang, B. Tang and Z. Li, *Sci. Adv.*, 2022, **8**, eabl8392.
33 G. Yang, S. Hao, X. Deng, X. Song, B. Sun, W. Hyun, M. Li and L. Dang, *Nat. Commun.*, 2024, **15**, 4674.
34 Y. Cai, Z. Wang, Y. Cui, X. Chen, G. Yang, H. Ou, H. Yuan and W. Yuan, *Adv. Mater.*, 2026, **38**, e18820.
35 W. Guo, X. Wang, B. Zhou and K. Zhang, *Chem. Asian J.*, 2020, **15**, 3469–3474.
36 W. Hao, Y. Wang and M. Liu, *ACS Mater. Lett.*, 2024, **6**, 3487–3495.
37 Q. Wang, Q. Zhang, Q. Zhang, X. Li, C. Zhao, T. Xu, D. Qu and H. Tian, *Nat. Commun.*, 2020, **11**, 158.
38 A. Nicol, R. Kwok, C. Chen, W. Zhao, M. Chen, J. Qu and B. Tang, *J. Am. Chem. Soc.*, 2017, **139**, 14792–14799.
39 Y. Zhang, Y. Su, H. Wu, Z. Wang, C. Wang, Y. Zheng, X. Zheng, L. Gao, Q. Zhou, Y. Yang, X. Chen, C. Yang and Y. Zhao, *J. Am. Chem. Soc.*, 2021, **143**, 13675–13685.
40 M. Liu, B. Wu, S. Shen, H. Sun, X. Gu, S. Li, Z. Tang, J. Cheng, X. Ma, M. Zhang, Y. Xu and L. Zhu, *ACS Macro Lett.*, 2025, **14**, 93–100.
41 M. Wu, Y. Guan, P. Wang, T. Hao, J. Li, W. Yuan, J. Huang, P. Duan, P. Wang and H. Xie, *Adv. Funct. Mater.*, 2025, **35**, 2505113.
42 Y. Lei, W. Dai, Y. Tian, J. Yang, P. Li, J. Shi, B. Tong, Z. Cai and Y. Dong, *J. Phys. Chem. Lett.*, 2019, **10**, 6019–6025.
43 L. Zhou, S. Mu, L. Ma, P. Jiang, Z. He, J. Song and X. Ma, *ACS Mater. Lett.*, 2024, **6**, 5384–5391.
44 X. Yao, Z. Lin, X. Liu, H. Ma, X. Wang, W. Huang and Z. An, *Angew. Chem., Int. Ed.*, 2025, **64**, e202510153.
45 S. Jia, B. Yang, J. Zhang, Y. Zhang, J. Wei, J. Du, M. Shan, J. Tang, W. Tang and J. Gong, *Small*, 2025, **21**, 2505073.
46 H. Liang, L. Yang, J. Cheng, T. Li, D. Zhang and Z. Xu, *Adv. Funct. Mater.*, 2026, **36**, e13575.
47 C. Yang and B. Yan, *ACS Appl. Mater. Interfaces*, 2025, **17**, 34219–34229.
48 X. Piao, T. Wang, X. Chen, G. Wang, X. Zhai and K. Zhang, *Nat. Commun.*, 2025, **16**, 868.
49 H. Yang, Y. Wang, Y. Wang, Z. Zhang, H. Ma, Y. Yamauchi, K. Ling, Y. Zhao, S. Cai, Z. An and W. Huang, *Adv. Mater.*, 2025, **37**, e03550.
50 Z. Yin, Z. Wu and B. Liu, *Adv. Mater.*, 2025, **37**, 2506549.
51 Z. Deng, J. Zhang, J. Zhou, W. Shen, Y. Zuo, J. Wang, S. Yang, J. Liu, Y. Chen, C. Chen, G. Jia, P. Alam, J. W. Y. Lam and B. Z. Tang, *Adv. Mater.*, 2024, **36**, 2311384.
52 Z. Xu, Y. Huang, S. Sun, L. Ma, B. Ding, H. Tian and X. Ma, *Nature Commun.*, 2025, **16**, 9668.
53 C. Chen, Z. Chi, K. Chong, A. Batsanov, Z. Yang, Z. Mao, Z. Yang and B. Liu, *Nat. Mater.*, 2021, **20**, 175–180.
54 X. Bao, E. Ushakova, E. Liu, Z. Zhou, D. Li, D. Zhou, S. Qu and A. Rogach, *Nanoscale*, 2019, **11**, 14250–14255.
55 P. Jiang, B. Ding, J. Yao, L. Zhou, Z. He, Z. Huang, C. Yin, H. Tian and X. Ma, *Angew. Chem., Int. Ed.*, 2025, **64**, e202421036.
56 Y. Zhang, X. Chen, J. Xu, Q. Zhang, L. Gao, Z. Wang, L. Qu, K. Wang, Y. Li, Z. Cai, Y. Zhao and C. Yang, *J. Am. Chem. Soc.*, 2022, **144**, 6107–6117.
57 D. Wang, H. Wu, J. Gong, Y. Xiong, Q. Wu, Z. Zhao, L. Wang, D. Wang and B. Tang, *Mater. Horiz.*, 2022, **9**, 1081–1088.
58 G. Ye, Y. Yang, W. Yuan, J. Gu, S. Li, Q. Li and Z. Li, *ACS Mater. Lett.*, 2024, **6**, 4639–4648.
59 M. A. El-Sayed, *J. Chem. Phys.*, 1963, **38**, 2834–2838.
60 X. Li, W. Li, Z. Deng, X. Ou, F. Gao, S. He, X. Li, Z. Qiu, R. Kwok, J. Sun, D. Phillips, J. Lam, Z. Guo and B. Tang, *J. Am. Chem. Soc.*, 2025, **147**, 14198–14210.
61 Y. Zhu, Y. Guan, Y. Niu, P. Wang, R. Chen, Y. Wang, P. Wang and H. Xie, *Adv. Optical Mater.*, 2021, **9**, 2100782.
62 H. Sun, Y. Xiao, Y. He, X. Wei, J. Zou, Y. Luo, Y. Wu, J. Zhao, V. Au and T. Yu, *Chem. Sci.*, 2025, **16**, 5299–5309.
63 J. Bai, L. Han, Y. Liu, L. Bu, S. Hu, J. Ma, Z. Li, M. Chen, Z. Ma and Z. Ma, *Adv. Funct. Mater.*, 2025, **35**, 2411496.